Journal of Hazardous Materials 169 (2009) 182–189

Contents lists available at ScienceDirect

Journal of Hazardous Materials

journal homepage: www.elsevier.com/locate/jhazmat

Air pollution effect of SO_2 and/or aliphatic hydrocarbons on marble statues in Archaeological Museums

T. Agelakopoulou, E. Metaxa, Ch.-S. Karagianni, F. Roubani-Kalantzopoulou*

School of Chemical Engineering, National Technical University of Athens, 9 Iroon Polytechniou St., 15780 Zografou, Athens, Greece

ARTICLE INFO

Article history:
Received 31 October 2008
Received in revised form 13 March 2009
Accepted 18 March 2009
Available online 27 March 2009

Keywords:
Deterioration of marble statues
Influence of pollutants on monuments
Synergistic hazardous effect
RF-IGC

ABSTRACT

This study allowed the identification of the main physicochemical characteristics of deterioration of the materials used in the construction of Greek ancient statues in order to plan a correct methodology of restoration. The method of Reversed-Flow Inverse Gas Chromatography is appropriate to investigate the influence of air pollutants on authentic pieces from the Greek Archaeological Museum of Kavala, near Salonica. Six local physicochemical quantities which refer to the influence of one or two pollutants (synergistic effect) were determined for each system. These quantities answer the question "when, why and how materials of cultural heritage are attacked".

1. Introduction

Air pollution can have a significant influence on the weathering of monuments and on the deterioration of museum objects [1]. The effects of several air pollutants on works of art have been reviewed and illustrated with examples in two European museums. The influence of tourism on the preservation of prehistoric rock art has also been addressed [2]. Sulfur dioxide is one of the most common pollutants of great interest concerning deterioration of marbles [3].

One of the largest single collections of outdoor sculpture and monuments in the United States is found at Gettysburg National Military Park, Pennsylvania. To assess the present status of monument deterioration and its relationship to airborne pollutants a research project has been conducted. Field measurements of the deterioration of weathered bronze plaques and marble obelisks that have been in place approximately 100 years have been made [4].

In Greece the interest concerning the conservation of monuments and artistic works of cultural heritage is enormous. The world known Parthenon on the old Acropolis of Athens and many other monuments made from the famous Pentelic marble as well a lot of statues of Archaeological Museums impose the investigation of the better conditions of conservation [5–8].

In two previous publications [9,10] a time resolved analysis has been presented in order to study the impact of some pollutant-gases on inorganic pigments of works of art. The proposed approach was experimental as well as through a model. The same chromatographic method can also be used successfully in measuring the damage of air pollution on monuments of cultural heritage. It is a flow perturbation method, namely the Reversed-Flow Inverse Gas Chromatography one and consists of reversing the direction of flow of the carrier gas from time to time. Then, the flow reversals create perturbations on the baseline of the chromatogram, having the form of extra chromatographic peaks. If the concentration of a substance in the flowing carrier gas depends on a rate process (i.e. slow diffusion), or on a fast process leading to an equilibrium state, then, one performs, through repeatedly reversing of flow, a repeated measurement of kinetic or thermodynamic parameters of this process [11–13].

Reversed-Flow Inverse Gas Chromatography (RF-IGC) has been used to study different phenomena and determine a series of physicochemical quantities [6,7,14–20]. This work falls within the scope of the investigation of degradation phenomena concerning building and cultural heritage materials, focused its attention on studying the degradation–conservation of two marble statues of Greek Archaeological Museum, that of Kavala near Salonica. It should be noted that a part of results from this research has recently been published in the same journal [21]. The examined systems are the following: $C_2H_6/(SO_2)$/L291 Statue of Kavala, $C_2H_4/(SO_2)$/L291 Statue of Kavala, $C_2H_2/(SO_2)$/L291 Statue of Kavala, $C_2H_6/(SO_2)$/L351 Statue of Kavala, $C_2H_4/(SO_2)$/L351 Statue of Kavala, $C_2H_2/(SO_2)$/L351 Statue of Kavala.

2. Experimental

The experimental set-up [11–13] is very simple and needs only a modification of a conventional gas chromatograph with a flame

* Corresponding author. Tel.: +30 210 77 23 277; fax: +30 210 20 27 691.
E-mail address: roubanif@central.ntua.gr (F. Roubani-Kalantzopoulou).

0304-3894/$ – see front matter © 2009 Elsevier B.V. All rights reserved.
doi:10.1016/j.jhazmat.2009.03.087

ionization detector. Inside the chromatographic oven of the Shimadzu GC-8A, were contained the sampling column, empty of any packing material, consisting of two sections and the diffusion column consisting also of two other sections. The reversing of the flow is effected by means of a valve. After injecting a small quantity of solute into the diffusion column as a pulse an asymmetrical concentration–time curve was recorded. When the carrier gas was restored to its original direction, extra chromatographic peaks were recorded corresponding to various experimental times.

The procedure was the following. The adsorbent (sample of statue) was packed in the diffusion column made of pyrex glass. The section, which was empty of any solid material, had a length of 22.0 cm, while the one containing the solid bed was 4.5 cm long. Both sections were of pyrex glass of a ID 3.5 mm. A small quantity of ethane or ethylene or acetylene (1.0 cm^3) was injected into the diffusion column. In the experiments for the synergistic effects of SO_2, this pollutant was injected as a 0.2 cm^3 pulse through the same column. A conditioning *in situ* at 423.2 K, under continuous flow of carrier gas, for 24 h, took place before each experiment. The carrier gas in all cases was nitrogen with a volumetric flow rate of 26.0 cm^3 min^{-1}. Both, the working temperature of the FID detector and the oven temperature were 323.2 K, as the summer temperature in Greece is high. The sampling column of total length of 100 cm was of stainless steel chromatographic tube of 4.0 mm ID.

3. Results and discussion

3.1. Time resolved analysis of all calculated physicochemical quantities

A time-resolved analysis has been done, the results of which are presented analytically. Seven indicative figures (Figs. 1–7) show the impact of hydrocarbons with or without SO_2, in physicochemical terms. Seven local physicochemical quantities have been determined namely, local adsorption isotherm θ, local adsorption energy ε, distribution function of adsorption energy $\varphi(\varepsilon;t)$, non-adsorbed gas concentration c_y, adsorbed gas concentration c_s^*, local monolayer capacity $c_{s\,max}^*$, entropy of adsorption ΔS. The used PC program is available upon request.

3.1.1. Statue L291, a pure calcite from the exterior of the Archaeological Museum of Kavala

(a) C_2H_2, C_2H_2/SO_2

From the curve of θ (Fig. 1), without the presence of SO_2, instant desorption in a very short time period is observed, in addition to a new, small reappearance of adsorption. With the presence of SO_2, desorption occurs more smoothly [22,23]. The physical meaning of high θ-values is that there

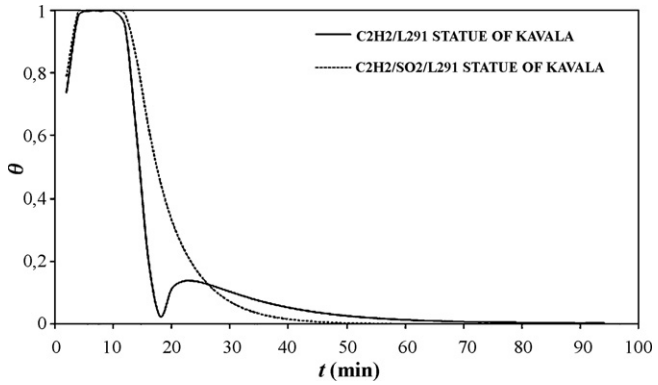

Fig. 1. Plot of local adsorption isotherm θ through a time resolved analysis for the system $C_2H_2/(SO_2)$/L291 Statue of Kavala.

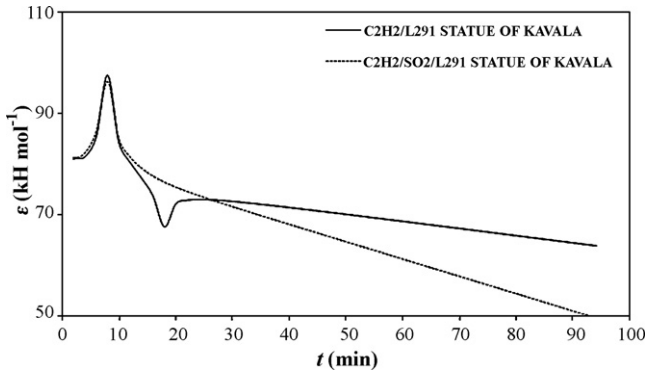

Fig. 2. Plot of local adsorption energy ε through a time resolved analysis for the system $C_2H_2/(SO_2)$/L291 Statue of Kavala.

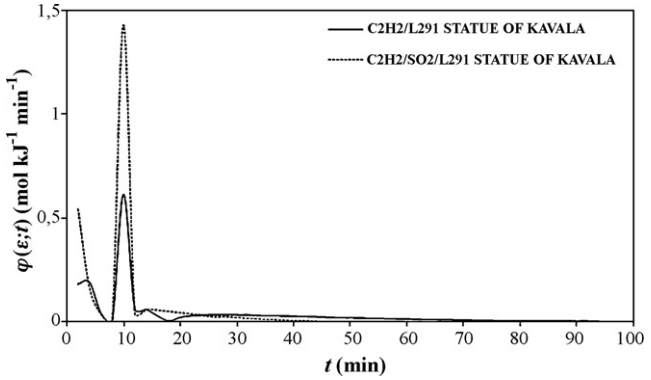

Fig. 3. Plot of distribution function of adsorption energy $\phi(\varepsilon;t)$ through a time resolved analysis for the system $C_2H_2/(SO_2)$/L291 Statue of Kavala.

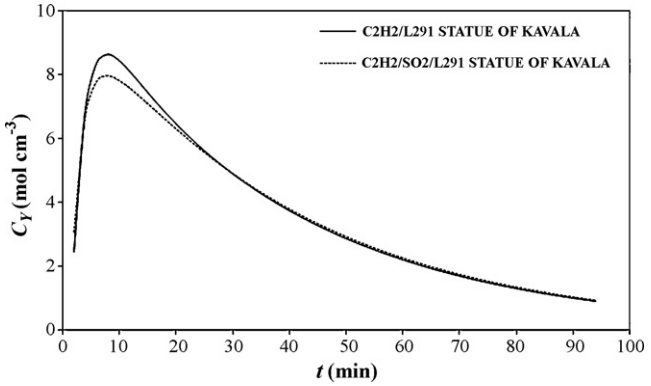

Fig. 4. Plot of non-adsorbed gas concentration c_y through a time resolved analysis for the system $C_2H_2/(SO_2)$/L291 Statue of Kavala.

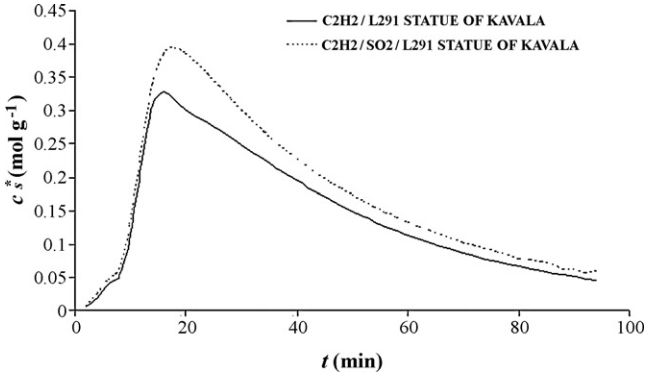

Fig. 5. Plot of local adsorbed gas concentration c_s^* through a time resolved analysis for the system $C_2H_2/(SO_2)$/L291 Statue of Kavala.

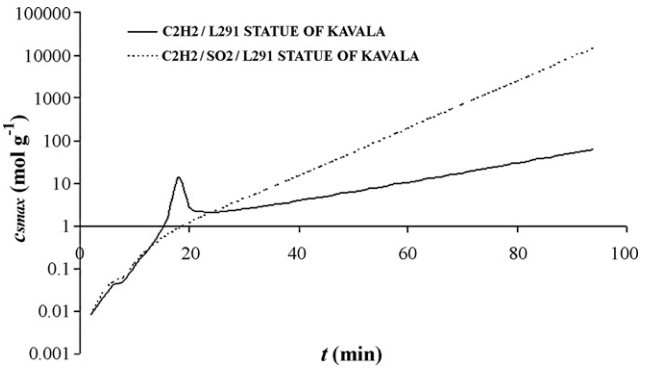

Fig. 6. Plot of local monolayer capacity $c^*_{s\max}$ through a time resolved analysis for the system $C_2H_2/(SO_2)$/L291 Statue of Kavala.

are stronger adsorbate–adsorbent interactions and random topography, instead of active sites of lower θ-values, where a coexistence and/or a competition of interactions between adsorbate–adsorbent and adsorbate–adsorbate determine the topography (patchwise and/or islands) of admolecules. The role of lateral molecular interactions between neighbor adsorbates greatly affects the kinetics of primary surface processes. Adsorbate aggregation, island formation, the appearance of different overlayer structures and phase transitions between them are among the mesoscopic manifestations of adsorbate lateral interactions. All of these phenomena affect the local environment of the adsorbed particles and are thus expected to significantly affect the kinetics of the various surface processes, such as diffusion, desorption, adsorption and/or chemical reaction. In every case, there is a complete correspondence between regions in plots $\varepsilon = \varepsilon(t)$ and $\theta = \theta(t)$ [24].

From the curve of ε (Fig. 2), the width of the energy values decreases with the presence of SO_2, from 69–98 kJ mol^{-1} to 81–98 kJ mol^{-1}. In this case, three areas of active sites appear, on the curves of $\varphi(\varepsilon;t)$ (Fig. 3), in addition to an increase of the maxima with the presence of SO_2. The first maximum from 0.19 mol kJ^{-1} min^{-1} becomes 0.55 mol kJ^{-1} min^{-1}, the second maximum from 0.62 mol kJ^{-1} min^{-1} becomes 1.43 mol kJ^{-1} min^{-1} and the third one shows a small increase.

Therefore, a synergy effect between SO_2 and C_2H_2 is obvious.

A slight decrease on the maximum of the curve of c_y (Fig. 4) with the presence of SO_2 is observed, from 8.6 mol cm^{-3} to 8 mol cm^{-3}. This is justified by the presence of SO_2.

With the absence of SO_2 a maximum on the curve of $c^*_{s\max}$ (Fig. 6) appears at 18 min, which disappears with the presence of SO_2. This denotes that the active sights are first occupied by the molecules of SO_2. Furthermore, an increase of the final maximum at a shorter time is observed.

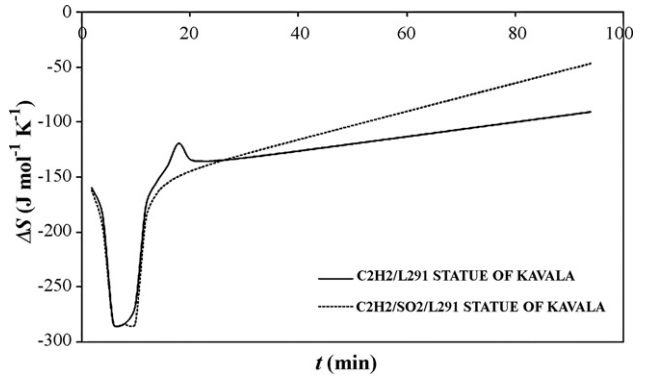

Fig. 7. Plot of entropy of adsorption ΔS through a time resolved analysis for the system $C_2H_2/(SO_2)$/L291 Statue of Kavala.

On the curve of the adsorption entropy, ΔS (Fig. 7), there is a coincidence of the maxima–minima, in addition to the appearance of a maximum at 18 min. It is noteworthy to observe that the descending part of the curve of ΔS describes adsorption, as at that point there is a decrease in the disorder due to the fact that some degrees of freedom of translational and rotational movement of the adsorbed molecules disappear. In a respective way, the ascending part describes desorption. Specifically, in Fig. 6, the slope of the curve on the part of desorption becomes bigger with the presence of SO_2.

Either from the aspect of adsorption–desorption or the view of different kinds of adsorbate–adsorbent and adsorbate–adsorbate interactions, the corresponding descending and ascending parts of these plots represent the decrease and increase, respectively, of degrees of freedom of molecules on adsorption and desorption processes, compared to them in the gas phase. The different surface topography reflects to admolecules with different mobilities on the various active sites, namely, with different degrees of freedom, in the sense that the different energy of each active site reflects to different binding strength towards the adsorbates and of course, to different mobility of adsorbates on the solid surface.

It is noted that the minimum on the curve of θ appears at the same time as the minimum on the curve of ε, the maximum on the curve of $c^*_{s\max}$ and the maximum of ΔS, with the absence of SO_2.

(b) C_2H_4, C_2H_4/SO_2

On the graph of θ (analogous to Fig. 1), desorption occurs nearly instantly without the presence of SO_2 in a very short time from the beginning of the experiment, while with the presence of SO_2 desorption occurs more smoothly.

As far as ε is concerned, a decrease is indicated in the width of the energy values, from 67–93 kJ mol^{-1} with the absence of SO_2 to 82–93 kJ mol^{-1} with the presence of SO_2.

Three distinctive areas of active sites appear on the corresponding diagram of $\varphi(\varepsilon;t)$, in addition to an increase of the peaks with the presence of SO_2 (the first maximum from 0.24 mol kJ^{-1} min^{-1} to 0.37 mol kJ^{-1} min^{-1}, the second one from 0.06 mol kJ^{-1} min^{-1} to 0.13 mol kJ^{-1} min^{-1} and the third maximum maintains the same value). Again a synergy effect is observed between SO_2 and C_2H_4, as in case (a).

A decrease in the maximum on the diagram of c_y is observed with the presence of SO_2 from 7.6 mol cm^{-3} to 6.9 mol cm^{-3}. It is the same behavior as noted in case (a) above.

On the curve of $c^*_{s\max}$ a peak appears at 24 min which disappears with the presence of SO_2, in addition to a decrease in the final maximum with the presence of SO_2 from 8.5×10^{-3} mol g^{-1} to 2.5×10^{-3} mol g^{-1}. The same explanation as in the relevant case of (a) above is valid.

With the absence of SO_2, on the graph of adsorption entropy, a maximum appears after the minimum of the adsorption curve. Furthermore, with the presence of SO_2 the slope of the curve decreases and the minimum changes from −2.85 J mol^{-1} K^{-1} to −2.90 J mol^{-1} K^{-1}.

(c) C_2H_6, C_2H_6/SO_2

A coincidence in the curves which describe the percentage of surface coverage, θ, is observed for the specific statue with the presence or absence of SO_2.

The reduction in the width of the energy values is slight (it is 82–98 kJ mol^{-1} with the absence of SO_2 and it becomes 82–94 kJ mol^{-1} with the presence of SO_2).

There are three areas of active sites also observed on the corresponding diagram of $\varphi(\varepsilon;t)$. The decrease in the first maximum is slight (from 0.4 mol kJ^{-1} min^{-1} to 0.3 mol kJ^{-1} min^{-1}), whereas

a very high increase is observed on the second maximum (from 0.13 mol kJ^{-1} min^{-1} to 9 mol kJ^{-1} min^{-1}).

There is absolute coincidence in the curves of c_y in the presence and absence of SO_2. In contrast, at the curves of $c^*_{s\,max}$ a time delay in maximum appearance is obvious in the presence of SO_2.

This case of adsorption differs from the other two above cases: (a) and (b).

On the curves of ΔS there is a coincidence of the maximum–minimum with a slight decrease in the slope of the curve with the presence of SO_2.

3.1.2. *Statue L351, a pure dolomite from the interior of the Archaeological Museum of Kavala*

(a) C_2H_2, C_2H_2/SO_2

Two curves which describe θ present near coincidence, while coincidence is observed in the range of the energy values (81–96 kJ mol^{-1}), with the presence of SO_2. The slope of the curve is more abrupt after the maximum which may be contributed to a more abrupt desorption.

Three clearly distinguishable areas of adsorption are observed on diagram of $\varphi(\varepsilon;t)$, where the first maximum increases from 0.18 mol kJ^{-1} min^{-1} to 0.55 mol kJ^{-1} min^{-1}, the second maximum remains stable at 0.15 mol kJ^{-1} min^{-1} and the third, although it remains at the same value, corresponds to a larger surface area in the presence of SO_2. As a consequence, a high degree of chemisorption appears [7].

Although the reported results regard experiments have been done at relatively low temperatures, where physisorption is more expected, the structural materials of samples of the statues used are energetically upgraded, as a consequence of the whole process they have been undergone from the moment of their natural formation until the moment of their use as a material for making statues. Thus, in the presence of an aggressive environment a chemisorption process is favored. Moreover, one or/and the other kind of adsorption processes take place in a various extent, because of the development of molecular lateral interactions (attractive or/and repulsive), in addition to the adsorbent–adsorbate interactions. In the specific case of chemisorption, repulsion effects prevail, resulting in random topography. By means of RF-IGC, chemisorption takes place in the beginning of our experiments (group A), as the ε-values indicate (cf. Figs. 2 and 9). At the same time, high θ-values are observed (cf. Figs. 1 and 8). The adsorbent–adsorbate interactions leading to chemisorption are chemical bond forces. Moreover, new active sites (groups B and C) are created by attractive lateral interactions with already adsorbed molecules. These new active sites are not on a free surface, but correspond to saddle points of adsorption potential, surrounded by other tightly adsorbed species (maybe, chemisorbed species), which support molecules on those points. Groups B and C correspond to lower surface coverage, as RF-IGC results show, resulting in a patchwise or/and island topography of the admolecules, determined by a coexistence of interactions between adsorbate–adsorbent and adsorbate–adsorbate. At this point, it must be pointed out that the former are forces leading to chemical bond formation and the latter ones are weak forces of Van der Waals type, which are responsible for physisorption [25].

Accordingly to Velasko and Rezzano studies [26], surface reconstruction process favors the formation of islands owing to attractive lateral interactions. Their results are in agreement with ours made by RF-IGC method, at higher time values and after $\theta = 1$, at saddle-points positions. Thus, desorption at higher time values outcomes from these islands due to steric effects between the nearest of them [27], without high energy demands.

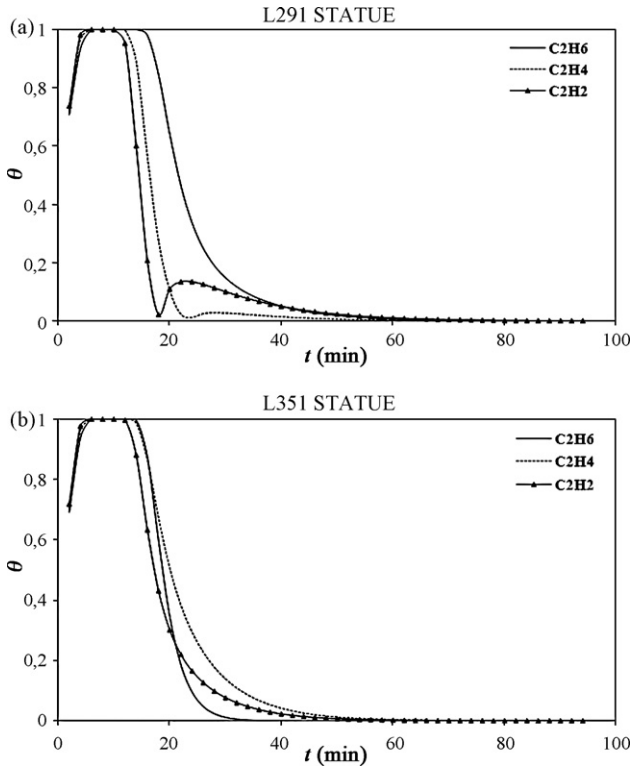

Fig. 8. Time resolved analysis of local adsorption isotherm θ for the systems: (a) C_xH_y/L291 Statue of Kavala and (b) C_xH_y/L351 Statue of Kavala.

The curves of c_y present the same behavior as in the corresponding case of statue L291 with a decrease of the maximum with the presence of SO_2.

On the corresponding diagram of $c^*_{s\,max}$ a time acceleration of the experiment is obvious with the presence of SO_2, in addition to an increase in the final maximum.

A coincidence of the curves which represent the ΔS is observed with a slight increase of the slope of the curve after 34 min, with the presence of SO_2.

(b) C_2H_4, C_2H_4/SO_2

A coincidence of curves is observed for θ, again with the absence or presence of SO_2.

In parallel, in the curves of ε, an increase in the width of energy values with the presence of SO_2 is observed, from 82–91 kJ mol^{-1} to 82–96 kJ mol^{-1}.

Three clearly distinguishable areas of active sites appear on the curves of $\varphi(\varepsilon;t)$. A time delay between the peaks of the curves of $\varphi(\varepsilon;t)$ is not observed, but an increase of the peaks with the presence of SO_2 is noted, more specifically, the first maximum from 0.2 mol kJ^{-1} min^{-1} becomes 0.5 mol kJ^{-1} min^{-1}, the second maximum from 0.4 mol kJ^{-1} min^{-1} becomes 0.46 mol kJ^{-1} min^{-1} and the third is similar with the corresponding case above.

An analogous behavior to the case of C_2H_2/SO_2 of the curves of c_y is observed with the absence or presence of SO_2. Moreover, the presence of SO_2 causes slight time acceleration of the experiment and an increase in the final maximum of the curve of $c^*_{s\,max}$ (from 32×10^{-3} mol g^{-1} to 72×10^{-3} mol g^{-1}).

As far as entropy of adsorption, ΔS, is concerned, a complete coincidence of the curves with the absence or presence of SO_2 is observed.

(c) C_2H_6, C_2H_6/SO_2

The curves which represent θ are of the same type with the presence or the absence of SO_2, with the difference that with the presence of SO_2 a time delay is obvious, which indicates slower desorption.

A decrease in the range of the energy values is realized with the presence of SO_2, from 55–97 kJ mol^{-1} to 83–94 kJ mol^{-1}, while at the same time a minimum appears at 38 min with the absence of SO_2.

Three areas of active sites appear again on the curve of $\varphi(\varepsilon;t)$. In the first maximum, a slight decrease from 0.30 mol kJ^{-1} min^{-1} to 0.27 mol kJ^{-1} min^{-1} is observed, while a very high increase of the second maximum from 0.44 mol kJ^{-1} min^{-1} to 80 mol kJ^{-1} min^{-1}is noted, in the presence of SO_2. The third region remains nearly constant. The high increase of the second peak is indicative of intense physisorption.

A slight decrease in the maximum of the curve of c_y with the presence of SO_2, from 6.9 mol cm^{-3} to 6.6 mol cm^{-3} is observed.

On the curve of $c^*_{s\,max}$, with the absence of SO_2 a maximum appears at 38 min with a value of 114×10^{-3} mol g^{-1}, which disappears in the presence of SO_2. That means that SO_2 molecules are first adsorbed on the statue.

On the curve of entropy of adsorption, ΔS, a coincidence of the maximum and minimum is again observed, in addition to the appearance of a new maximum at 38 min with the absence of SO_2.

3.2. Conclusions concerning the effect of the bond of hydrocarbon

The kind of the bond is carefully examined studying all physicochemical quantities obtained. Seven figures (Figs. 8–14) show this effect.

3.2.1. Local adsorption isotherm

On the statue L291, which is calcite, (Fig. 8a), acetylene seems to be desorbed first with an abrupt desorption at 18 min. Ethylene follows with a less abrupt desorption at 24 min and last ethane with a smoother desorption.

In contrast, on the statue L351, which is dolomite, (Fig. 8b), the slopes of the descending branches concerning desorption, are initially similar for the three hydrocarbons. Moreover, the desorption is completed first for ethane at 28 min and follow acetylene and ethylene. The bigger experimental times of desorption in this case are justified by the greater porosity of dolomite.

3.2.2. Local adsorption energy

In the case of statue L291 (Fig. 9a), the same form of curve is observed for all three hydrocarbons. The same range of energy values apply to ethylene and acetylene but ethane varies.

A coincidence of curves is observed in the case of the statue L351 (Fig. 9b), with ethylene and acetylene to present the same behavior. Ethane varies, presenting a minimum on the curve at 38 min.

3.2.3. Distribution function of adsorption energy

In the case of both statues, three distinct areas of active sites of adsorption appear.

Specifically, on the statue L291 (Fig. 10a), in the first region, ethane seems to be adsorbed at a greater percentage. The percentage of adsorption active sites, in this area, follows the order: $C_2H_6 > C_2H_4 > C_2H_2$. In the second area of active sites, the greater extent of adsorption corresponds to acetylene and follows ethane and ethylene.

On the statue L351 (Fig. 10b), in both categories of active sites adsorption follows the order: $C_2H_6 > C_2H_4 > C_2H_2$.

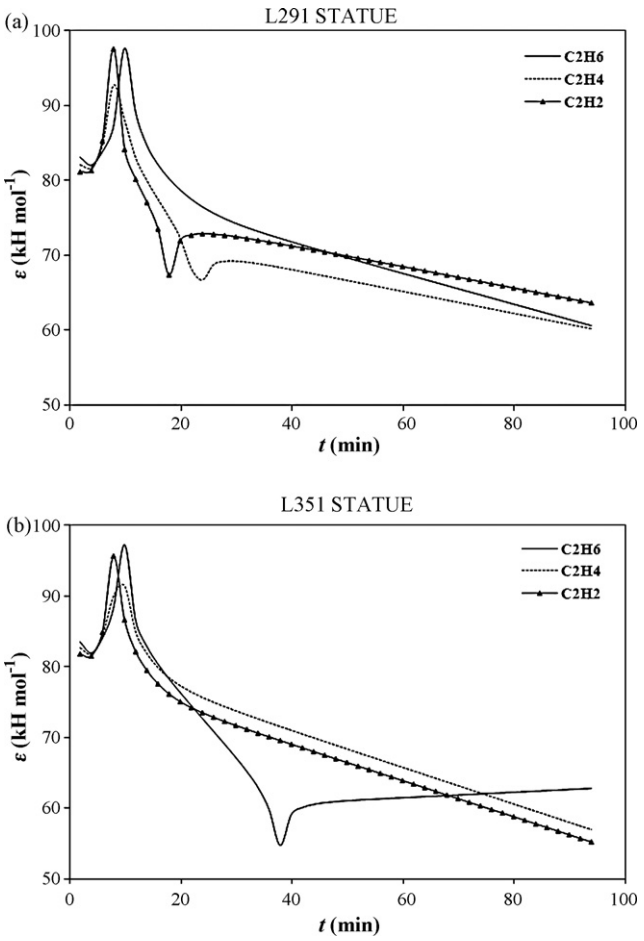

Fig. 9. Time resolved analysis of local adsorption energy ε for the systems: (a) C_xH_y/L291 Statue of Kavala and (b) C_xH_y/L351 Statue of Kavala.

3.2.4. Non-adsorbed and adsorbed concentration of pollutant

It must be noted that the type of bond affects the behavior of both statues in the same way (Fig. 11). Specifically, the non-adsorbed hydrocarbon concentration is lesser for ethane, followed by ethylene and then acetylene. Therefore:

$$\text{non-adsorbed}\,C_2H_6 < \text{non-adsorbed}\,C_2H_4 < \text{non-adsorbed}\,C_2H_2$$

3.2.5. Local monolayer capacity

From Fig. 13, it is obvious that the dolomite statue presents higher local monolayer capacities in all three cases instead of calcite statue. Specifically, for dolomite the order of c_{smax} is $C_2H_6 \gg C_2H_2 > C_2H_4$. In contrast, for calcite the corresponding values of c_{smax} are much lesser and the order is $C_2H_4 > C_2H_2 > C_2H_6$ until 30 min and then becomes $C_2H_4 > C_2H_6 > C_2H_2$.

The observation that the maximum final value of c_{smax} for the statue L351 is 120×10^{-3} mol g^{-1}, while for the statue L291 is too small, which can be attributed to the origin of the statue, is noteworthy. The statue L351, as mentioned above, is dolomite and has larger porosity compared to the statue L291, which is calcite, a fact which explains its greater adsorption.

The amounts of the adsorbed hydrocarbons c_s have been calculated, both in the absence and presence of SO_2. These data are summarized in Table 1.

As regards L291 Statue of Kavala, the effect of the bond of hydrocarbon is clearly remarked. To be specific, the estimated total amount of adsorbed hydrocarbon increases as the higher unsatu-

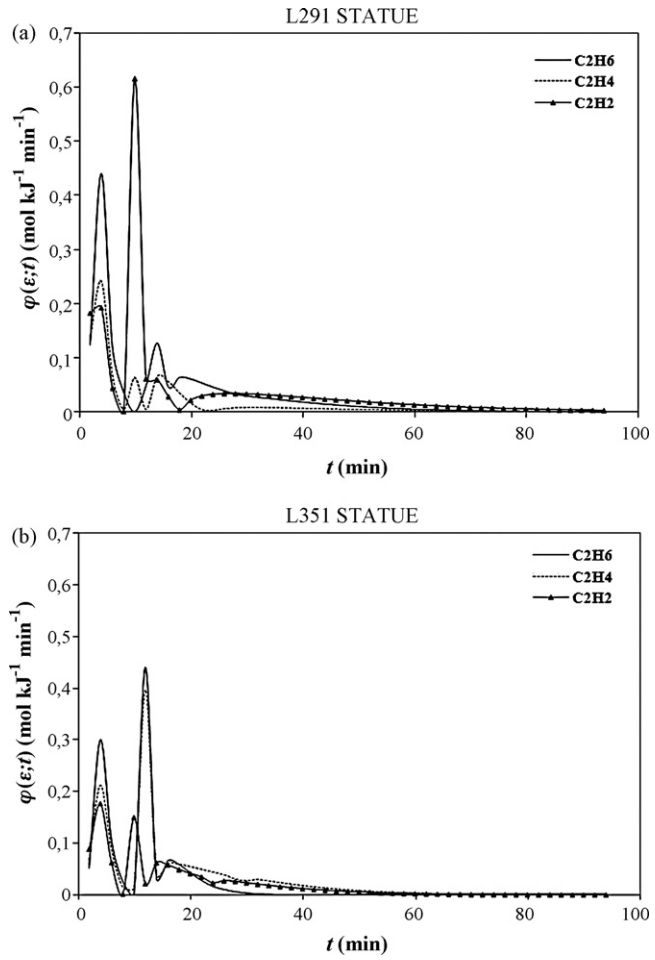

Fig. 10. Time resolved analysis of distribution function of adsorption energy $\phi(\varepsilon;t)$ for the systems: (a) C_xH_y/L291 Statue of Kavala and (b) C_xH_y/L351 Statue of Kavala.

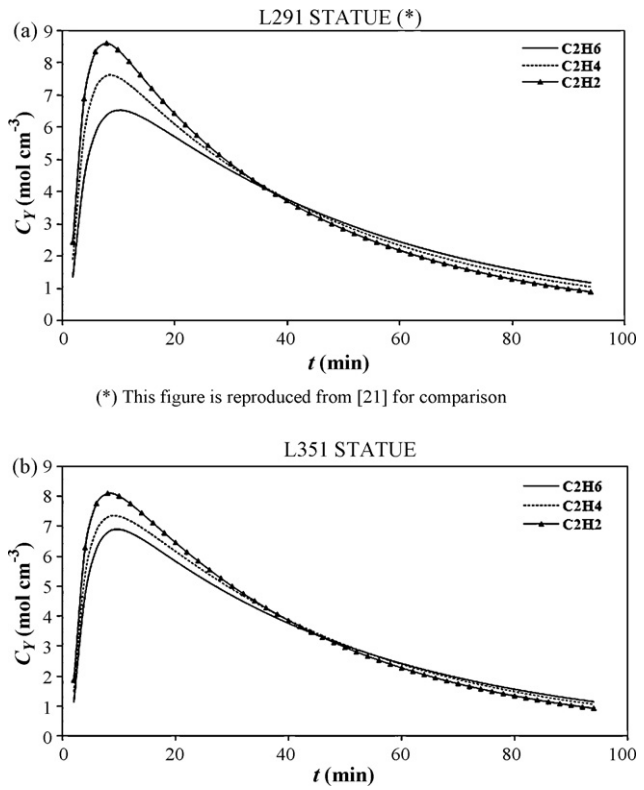

Fig. 11. Time resolved analysis of non-adsorbed gas concentration c_y for the systems: (a) C_xH_y/L291 Statue of Kavala and (b) C_xH_y/L351 Statue of Kavala.

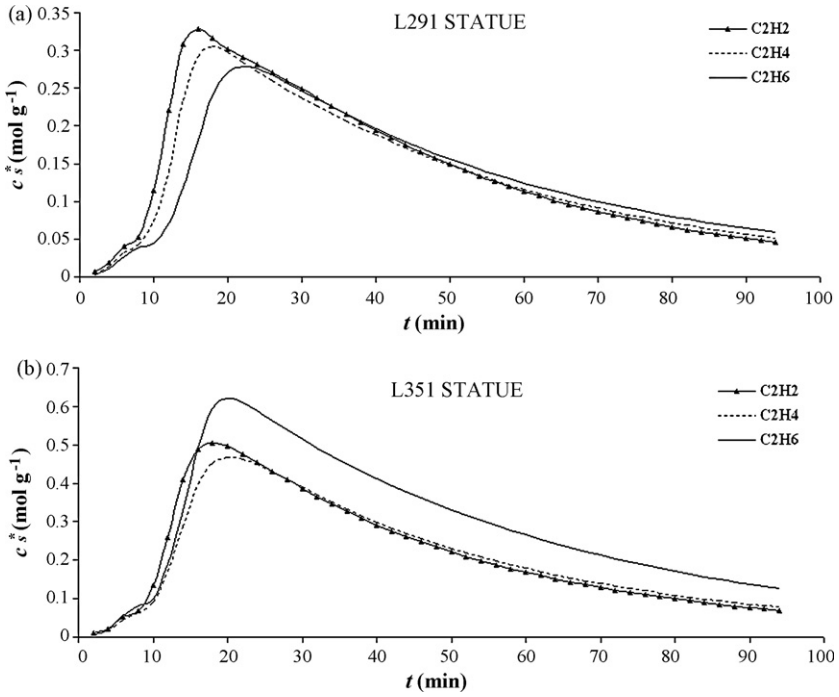

Fig. 12. Time resolved analysis of adsorbed gas concentration c_s^* for the systems: (a) C_xH_y/L291 Statue of Kavala and (b) C_xH_y/L351 Statue of Kavala.

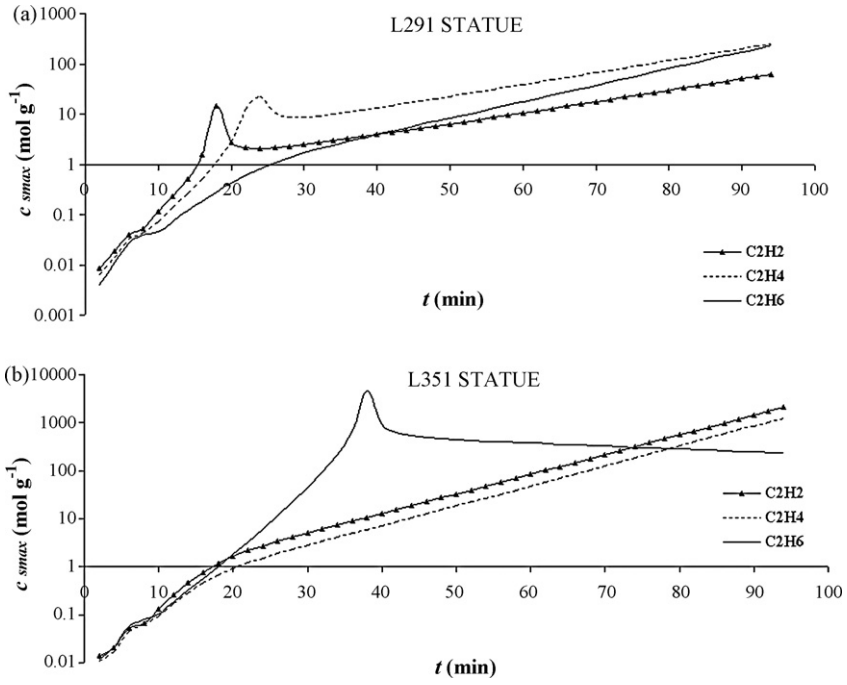

Fig. 13. Time resolved analysis of local monolayer capacity $c^*_{s\,\max}$ for the systems: (a) C_xH_y/L291 Statue of Kavala and (b) C_xH_y/L351 Statue of Kavala.

rated its bond is, with or without the presence of sulfur dioxide. Moreover, with the presence of sulfur dioxide, an increment of the estimated total amount of adsorbed acetylene is noted, contrary to the other hydrocarbons where the presence of sulfur dioxide causes only a negligible or no effect. That means, in the presence of sulfur dioxide the adsorption of acetylene on the statute surface is prolonged (positive synergistic effect) for a longer time interval than in the absence of it. A possible explanation for it could be that the active sites of the statue surface are first occupied by the molecules of sulfur dioxide, obstructing someway the adsorption of acetylene on it.

As regards L351 Statue of Kavala, the estimated total amount of each adsorbed hydrocarbon – either with or without the presence of sulfur dioxide – is higher than in case of L291 Statue of Kavala, a fact that is ascribable to the higher porosity of the former, which is dolomite, whereas the latter one is calcite. Furthermore, the synergistic effect of SO_2 is more profound in case of dolomite. For the same statue, the higher estimated adsorbed amount is found for ethane in the absence of SO_2, something is reversed in the presence of SO_2 and regards acetylene. In addition, the synergistic effect of SO_2 is on the decline from acetylene to ethylene and ethane. That means the order of the bond of hydrocarbon signifies more in the presence of sulfur dioxide.

Table 1
The estimated total amounts of adsorbed C_xH_y for every adsorption system $C_xH_y/(SO_2)$/Statue of Kavala (after integration of the corresponding functions, $c^*_s = c^*_s(t)$.

Adsorption system	$c^*_{s(tot.)}$ (mol g^{-1} s)
L291 Statue of Kavala	
C_2H_2	269.12
C_2H_2/SO_2	311.17
C_2H_4	242.73
C_2H_4/SO_2	242.73
C_2H_6	220.98
C_2H_6/SO_2	208.8
L 351 Statue of Kavala	
C_2H_2	405.6
C_2H_2/SO_2	442.4
C_2H_4	378.4
C_2H_4/SO_2	415.2
C_2H_6	504.0
C_2H_6/SO_2	341.2

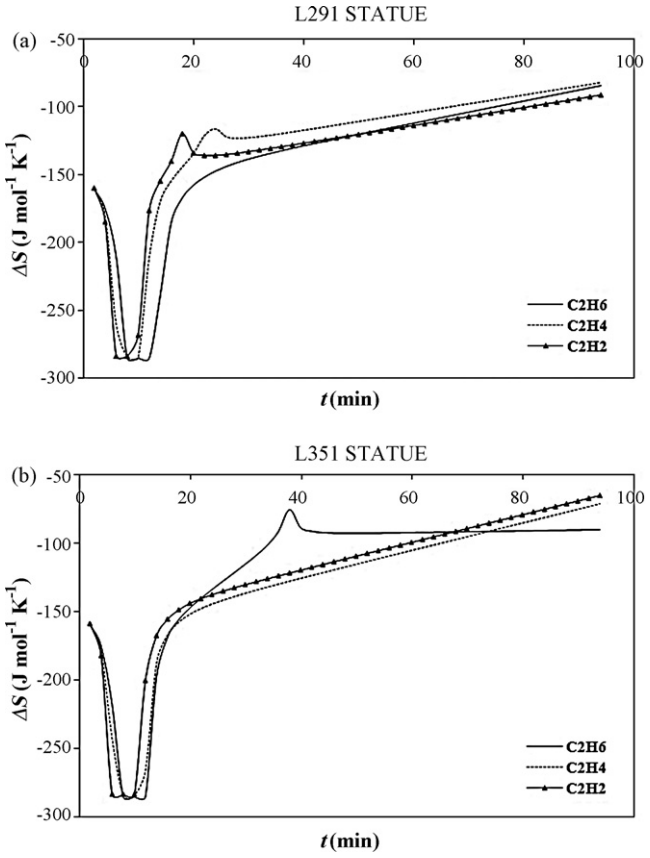

Fig. 14. Time resolved analysis of entropy of adsorption ΔS for the systems: (a) C_xH_y/L291 Statue of Kavala and (b) C_xH_y/L351 Statue of Kavala.

3.2.6. Entropy of adsorption

On both statues (Fig. 14), irrespective of hydrocarbon, a coincidence of the initial maximum ($-158\,J\,mol^{-1}\,K^{-1}$) and of the minimum ($-284\,J\,mol^{-1}\,K^{-1}$) is observed. Furthermore the ascending part of the curve of ΔS, which corresponds to desorption, varies only on ethane for the statue L351. An abrupt increase of entropy is observed, which confirms the existence of physisorption in this case, a fact that has been also concluded in the analysis of the corresponding distribution function of adsorption energy.

Acknowledgements

The authors acknowledge the financial support under the research program PYTHAGORAS II 2005–2007. The project is co-funded by the European Social Fund (75%) and National Resources (25%).

Special thanks to the Archaeological Museum of Kavala for the kindly supply of statue samples, by permission of Greek Ministry of Culture.

References

[1] P. Brimblecombe, in: J.N. Lester, R. Perry, G.L. Reynolds (Eds.), Quality of Air in the Museum Environment. Quality of the Indoor Environment, Selper Ltd., London, 1992.
[2] R.V. Grieken, F. Delalieux, K. Gysels, Cultural heritage and the environment, Pure Appl. Chem. 70 (1998) 2327–2331.
[3] T.T.N. Lan, Phoung Thoa Thi, R. Nishimura, Y. Tsujino, M. Yokoi, Y. Maeda, New model for the sulfation of marble by dry deposition sheltered marble—the indicator of air pollution by sulfur dioxide, Atmos. Environ. 39 (9) (2005) 913–920.
[4] D.A. Dolske, J.D. Meakin, Acid deposition impacts on historic bronze and marble statuary and monuments, Mater. Perform. 30 (1991) 53–57.
[5] E. Metaxa, E. Kalogirou, F. Roubani-Kalantzopoulou, A Physicochemical study of the influence of ethene and ethyne on various marbles, Rus. J. Phys. Chem. 73 (1999) 112–116.
[6] N.A. Katsanos, F. De Santis, A. Cordoba, F. Roubani-Kalantzopoulou, D. Pasella, Corrosive effects from the deposition of gaseous pollutants on surfaces of cultural and artistic value inside museums, J. Hazard. Mater. A 64 (1999) 21–36.
[7] N.A. Katsanos, E. Arvanitopoulou, F. Roubani-Kalantzopoulou, A. Kalantzopoulos, Time distribution of adsorption energies, local monolayer capacities, and local isotherms on heterogeneous surfaces by inverse gas chromatography, J. Phys. Chem. B 103 (1999) 1152–1157.
[8] F. Roubani-Kalantzopoulou, T. Agelakopoulou, I. Bassiotis, S. Margariti, V. Siokos, E. Metaxa, Influence of nitrogen dioxide and acetylene on marbles, ceramics and pigments, GNEST J. 10 (2008) 183.
[9] A. Kalantzopoulos, S. Birbatakou, F. Roubani-Kalantzopoulou, Benzene and toluene influence with or without nitrogen dioxide on inorganic pigments of works of art—Part I, Atmos. Environ. 32 (1998) 1811–1816.
[10] T. Agelakopoulou, I. Bassiotis, E. Metaxa, F. Roubani-Kalantzopoulou, Benzene and toluene influence with or without nitrogen dioxide on inorganic pigments of works of art—Part II, Atmos. Environ. 41 (2007) 2009–2018.
[11] N.A. Katsanos, Determination of chemical kinetic properties of heterogeneous catalysts, J. Chromatogr. A 1037 (2004) 125–145.
[12] F. Roubani-Kalantzopoulou, Determination of isotherms by gas–solid chromatography applications, J. Chromatogr. A 1037 (2004) 191–221.
[13] G. Karaiskakis, D. Gavril, Determination of diffusion coefficients by gas chromatography, J. Chromatogr. A 1037 (2004) 147–189.
[14] D. Gavril, A. Koliadima, G. Karaiskakis, Adsorption studies of gases on Pt–Rh bimetallic catalysts by Reversed–Flow Gas Chromatography, Langmuir 15 (1999) 3798–3806.
[15] F. Roubani-Kalantzopoulou, I. Bassiotis, Th. Artemiadi, S. Margariti, E. Arvanitopoulou, N.A. Katsanos, Simulation of the physicochemical processes in the atmosphere, Fresen. Environ. Bull. 10 (2001) 98–102.
[16] V. Siokos, J. Kapolos, F. Roubani-Kalantzopoulou, Physicochemical characterization of inorganic pigments in the presence of gaseous pollutants: the role of ozone, Z. Physik. Chem. 216 (2002) 1311–1321.
[17] S. Margariti, V. Siokos, F. Roubani-Kalantzopoulou, Experimental determination of adsorption energies, adsorption isotherms, probability density functions and lateral molecular interactions on C_XH_Y/CaO systems, J. Chromatogr. A 1018 (2003) 213–223.
[18] E. Metaxa, T. Agelakopoulou, I. Bassiotis, S. Margariti, V. Siokos, F. Roubani-Kalantzopoulou, Time-resolved gas chromatography applied to submonolayer adsorption: modelling and experimental approach, Appl. Surf. Sci. 253 (2007) 5841–5845.
[19] A. Giannoudakos, T. Agelakopoulou, I. Asteriadis, M. Kompitsas, F. Roubani-Kalantzopoulou, Development and characterization of ZnO, Au/ZnO and Pd/ZnO thin films through their adsorptive and catalytic properties, J. Chromatogr. A 1187 (2008) 216–225.
[20] T. Agelakopoulou, V. Floropoulou, E. Metaxa, F. Roubani-Kalantzopoulou, Ch. Karagianni, XRD–Raman–SEM analysis of marbles exposed to gas pollutants, submitted for publication.
[21] E. Metaxa, T. Agelakopoulou, I. Bassiotis, Ch.-S. Karagianni, F. Roubani-Kalantzopoulou, Gas chromatographic study of degradation phenomena concerning building and cultural heritage materials, J. Hazard. Mater. 164 (2009) 592–599.
[22] N.A. Katsanos, G. Karaiskakis, Time-Resolved Inverse Gas Chromatography and Its Applications, HNB Publishing, New York, 2004.
[23] N. Bakaoukas, A. Koliadima, L. Farmakis, G. Karaiskakis, N.A. Katsanos, Chromatographia 57 (2003) 783–791.
[24] I. Farbman, M. Asscher, A. Ben-Shaul, J. Chem. Phys. 104 (1996) 5674–5682.
[25] E. Metaxa, T. Agelakopoulou, Ch.-St. Karagianni, F. Roubani-Kalantzopoulou, Instrum. Sci. Technol., in press.
[26] P.A. Velasko, J.L. Rezzano, Influence of surface stress on reconstruction processes: analytical study and simulation by the Monte Carlo Method, J. Phys.: Condens. Matter 11 (1999) 4971–4984.
[27] F. Rahman, M. Kuroda, T. Kiyonaga, F. Khanom, H. Tsurumaki, S. Inanaga, Modulated hydrogen beam study of adsorption-induced desorption of deuterium from Si(1 0 0)-3×1:D Surfaces, J. Chem. Phys. 121 (2004) 3221–3227.